INFLUENCE OF TIP SHROUD CAVITIES ON LOW-PRESSURE TURBINE MAIN FLOW AT DESIGN AND OFF-DESIGN CONDITIONS

M. Perini[*†] *- N. Binder*[†] *- Y. Bousquet*[†] *- E. Schwartz*[*]

* Safran Aircraft Engines, Moissy-Cramayel, France
†Université de Toulouse, ISAE-Supaéro, Toulouse, France
Email : maxime.perini@isae-supaero.fr

ABSTRACT

A lot of studies on turbomachinery main flow optimisation have been performed in order to reach actual efficiency level of modern gas turbines. To go further in the study of aerodynamic losses sources, a better understanding on technological effects is required. Tip shroud cavities in low pressure turbine is an example. Indeed, the by-pass flow causes additional pressure losses. In addition, interactions between main flow and cavity flows, as well as the re-entering flow, cause mixing losses and modifications of flow angle. This paper investigates the contribution of tip shroud cavities in a low pressure turbine stage on flow structures using (Unsteady) Reynolds Averaged Navier-Stokes simulations. The ability of a steady simulation to predict the overall performance and flow physics of this kind of flow is well documented in the literature but time-resolved simulations are needed to deepen the analysis. This is an objective of this paper. Following the presentation of the configuration under investigation, an analysis of flow structures is made in the upstream region of the rotor, close to the shroud. After that, simulations at off-design conditions are studied in order to evaluate this impact on the previous mechanisms.

NOMENCLATURE

π_{tot} Total to total pressure ratio
η_{is} Isentropic efficiency
U Circonferential velocity of the rotor blade [m/s]
h_t Total enthalpy [J]
β Yaw angle in relative frame of reference [deg]
dt Time step [s]
BPF Blade passing frequency [Hz]
T Period of rotation [s]
RMS Root mean square
M_r Rotor exit Mach number
P Static pressure [Pa]
X Axial coordinate [m]
c_{ax} Axial chord [m]
ψ Stage loading

INTRODUCTION

Modern low pressure turbines have already reached high efficiency level thanks to main flow path and airfoils optimisation. One way to get improvements is to consider technological effects during the design process. Indeed, flows in the vicinity of technological effects are sources of losses and have to be optimised to increase efficiency. Shrouded blades used in low pressure turbine in order to minimise losses due to rotor tip leakage flow occurring in unshrouded turbines [1] is the one studied in this paper. Aerodynamic loss sources are of different types. The most important are pressure losses when bypass mass flow goes through seal gaps and mixing losses when it re-enters in the main flow [2, 3]. Also, interactions between inlet/outlet cavities

and main flow path create additional shear layers at interface and introduce modifications of flow angle leading to different work output and intensified secondary flows in the rows [4, 5]. In addition, interactions can be influenced by unsteadiness created by blade wakes and potential fields. Consequently time-resolved numerical simulations are required to understand theses processes and to identified improvements. The major part of research works that has been done on shrouded turbine is at design condition. Pressure losses are proportional to the mass flow rate as well as pressure ratio and mixing losses depend on the difference between main flow and leakage flow momentum [6]. That is why off-design conditions, modifying back pressure or rotational speed, may affect mechanisms and change the amount of generated losses.

This paper presents results from 3D unsteady numerical simulations on a one stage low pressure turbine. This case is adapted from a low speed, low pressure ratio and cold air test rig at Darmstatd university on which experimental data are available [7]. The paper has two main objectives. The first one is to show which mechanisms RANS simulations are able to capture or not. The second one is to demonstrate how off-design condition deteriorate a beneficial mechanism present at design condition. Flow features of the turbine at design condition are first presented. Then CFD computations are performed to investigate the behaviour of cavity/main flow interaction at off-design condition.

TEST CASE AND NUMERICAL SET UP

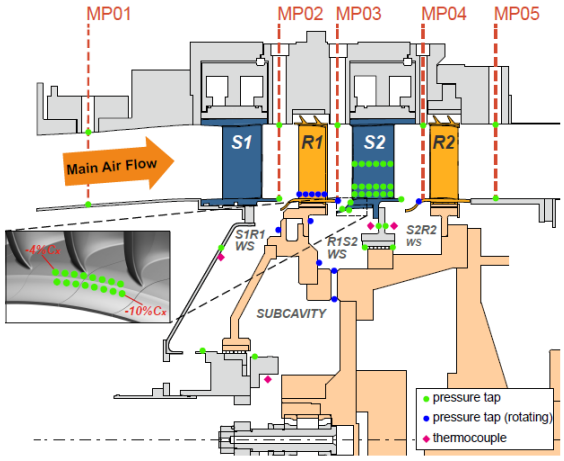

Figure 1: **Meridional view of MAGPI test rig (with instrumented planes), from [7]**

Rotation speed	766 rpm
Total to total pressure ratio	1.04
Rotor exit Mach number	0.19
Stator Reynolds number	5.10^5
Rotor Reynolds number	5.10^5

Table 1: **Test case specification**

The configuration under investigation is an experimental facility, in Darmstadt university (Germany), representing a high-diameter two-stage low pressure turbine equipped with a representative low pressure turbine blading set up [7]. Initially designed to study interaction between purge and main gas path, in the framework of European project MAGPI, this shrouded turbine has been chosen because of its available experimental data. Figure 1 illustrates a meridional view of the test rig. The main specification of the test rig are given in the Table 1. It can be noticed that pressure ratio and Mach number are lower than real engine stages. Also, the by-pass massflow rate, not measured experimentally but calculated with the simulations, corresponds to 1.5% of the main flow. It is a relatively high value compared to values cited in literature; generally between 0.4% and 1%. However, these features will permit to discuss and extend the conclusions drawn by authors previously cited.

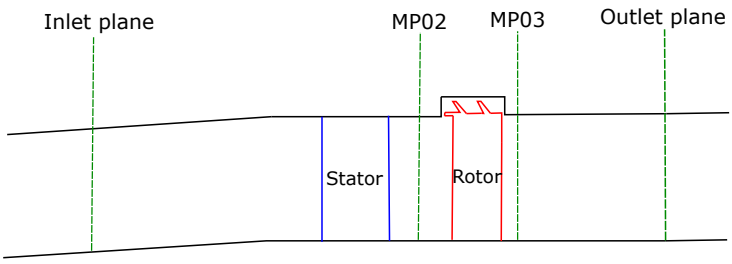

Figure 2: **Meridional view of the computational domain**

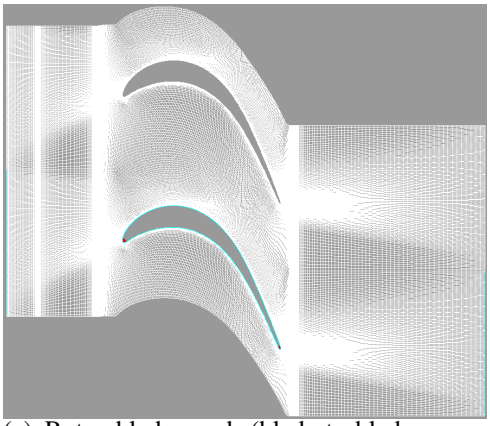

(a) Rotor blade mesh (blade-to-blade representation)

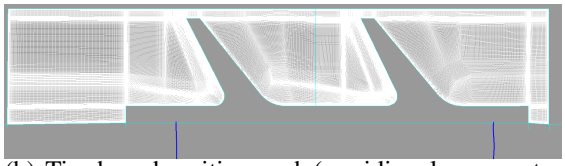

(b) Tip shroud cavities mesh (meridional representation)

Figure 3: **Blade-to-blade view of the rotor mesh (mid-span) and meridional view of cavities mesh**

Two geometries are studied in this paper to isolate main flow features modifications caused by tip shroud cavities. The first one, referred as "baseline", corresponds to an ideal rotor without tip gap. The rotor shroud is fixed in the relative frame of reference. The second one, referred as "cavities", corresponding to the real shrouded geometry. For computational cost reason, only the first stage of the turbine has been performed. Moreover, the generation of a structured mesh of such complex geometry can be time consuming. Considering that purge cavities have a limited impact on main flow properties above fifty percent of blade span [8], it has been chosen to remove purge cavities. Figure 2 gives a representation of the computational domain.

The mesh is represented in Figure 3. Connectivities between cavities and rotor blocks are fully matching. The size of the first cell is set to $5\mu m$ leading to $y^+ < 3$ in the near wall region. For each channel there are about 2.5 millions points in the stator, 6.5 millions in the rotor and 20 millions in tip shroud cavities. The same grid is used for all simulations.

Computations were performed using elsA code, developed by ONERA and CERFACS. It solves the three dimensional (Unsteady) Reynolds-Averaged Navier-Stokes equations based on cell-centred finite volume method on multi-block structured grids. Every simulations were done using $k - \omega$ Wilcox [9] turbulence model. Recent study, by Wein et al. [10], showed that the model is able to correctly predict the global discharge coefficient across the labyrinth seal. However, regarding flow structure inside inlet/outlet cavities, the model still presents some discrepancies compared to PIV measurements. Jameson's [11] second order centred scheme

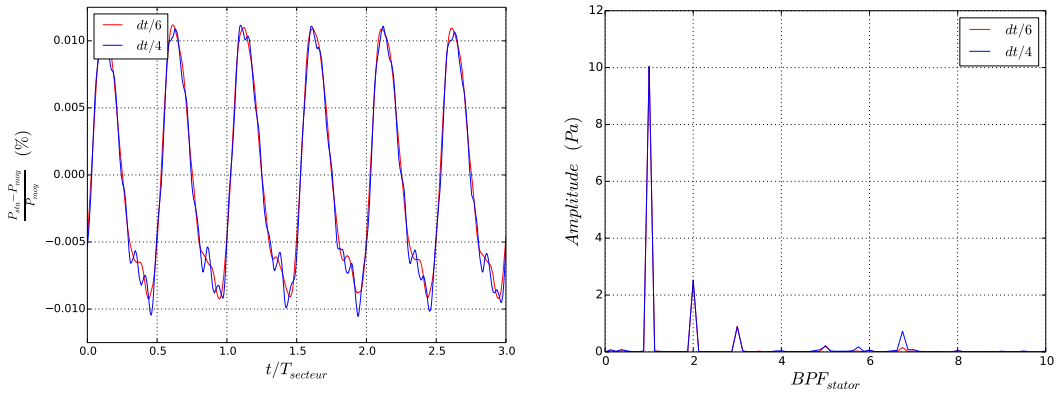

(a) Signal

(b) FFT spectrum

Figure 4: **Temporal evolution of static pressure from numerical probe at mid-span and upstream rotor blade leading edge. Fourier transform of the signal**

was used to compute convective fluxes and diffusive fluxes used second order centred scheme.

Inlet and outlet boundary conditions are the same for all simulations. At the inlet (MP01 plane), constant total pressure and total temperature are imposed as well as flow angle. At the outlet ($3c_{ax,rotor}$ downstream MP03 plane), a radial equilibrium law imposes a static pressure distribution. Walls are set to an adiabatic no-slip condition. For the steady simulations, the mixing plane approach is used at stator-rotor interface. In unsteady simulations, the azimuthal periodicity of the machine ($\frac{2\pi}{24}rad$) allows a reduction of the modelling domain such as two stator blades and three rotor blades are simulated on both sides of the interface. Finally, instantaneous periodic boundary conditions are used on azimuthal borders.

Steady computations were done using backward Euler time scheme while unsteady cases used Gear's second order scheme with sub-iterations. Convergence for steady simulations is assumed when residuals decrease reach three or five order of magnitude, depending on the residual quantity. For the unsteady simulations, convergence criteria is based on pressure signal periodicity extracted from numerical probes. Four different time steps values are investigated. The first one, noted dt discretise the rotor blade passing frequency by using 240 time steps. Other time steps values correspond to $dt/2$, $dt/4$ and $dt/6$. Simulations using dt and $dt/2$ are converged but non physical static pressure fluctuations of $1000Pa$ and between $3-10kHz$ are recorded on numerical probes. Only simulation using $dt/4$ and $dt/6$ lead to periodical signal of static pressure. Figure 4(a) shows temporal evolution of static pressure from a probe located near the rotor leading edge at mid-span. $dt/4$ case is represented with blue line and $dt/6$ case with red line. Figure 4(b) shows the Fourier transform of previous signals. The $dt/4$ case overestimate the amplitude of the mode around $6BPF_{stator}$. However, regarding this difference of amplitude it has been chosen to continue the study using the $dt/4$ time step corresponding to a physical time step $dt \sim 10^{-6}s$. Such a refined time resolution of the pitch is required since the characteristic time of a possible coupling between the cavity and the main flow is not based on rotor/stator interactions [12].

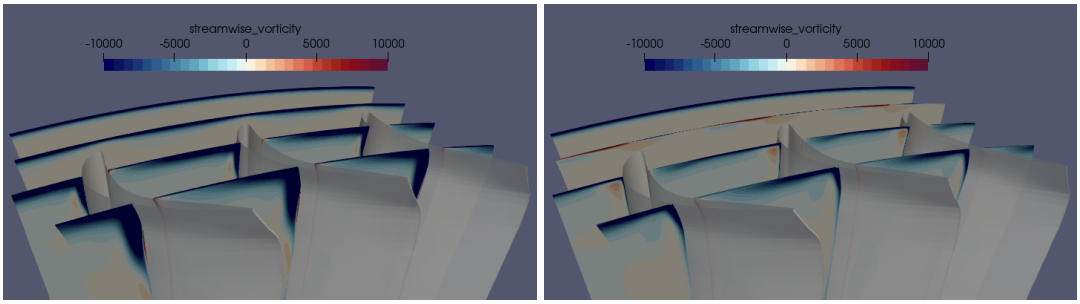

(a) Baseline (b) With cavities

Figure 5: **Axial cuts of streamwise vorticity along x-axis for baseline and cavity cases**

RESULTS

Validation of this numerical set up, at design condition, has already been done on a previous study thanks to the available experimental data [13]. Table 2 summarises stage performance for unsteady reference case and experimental data. Total torque measurement was done on the experimental facility to compute the two stages efficiency but, in our case, mean values of total pressure and total temperature on planes MP01 and MP03 are used to compute the first stage efficiency of MAGPI.

Table 2: **Global performance parameters**

	π_{tot}	$\psi = \frac{\Delta h_t}{U^2}$	η_{is}
Cavities URANS	1.042	2.02	0.902
MAGPI	1.043	2.04	0.91

(U)RANS predictability

The same study [13] showed that a large part of tip shroud cavities influence on global performance is well captured by RANS simulations. Changes in flow physics due to tip shroud cavities are also correctly predicted by steady simulations. One very interesting example is the reduction of passage vortex inside rotor channel. Figure 5 shows four axial cuts of streamwise vorticity inside the rotor domain for the baseline and cavities case : $3mm$ upstream and downstream the inlet cavity as well as at 10% and 30% axial rotor chord. On the upstream cavity plane, the negative streamwise vorticity zones correspond to the migration of shroud boundary layer from pressure side to suction side due to azimuthal pressure gradients. Starting from the second plane, downstream the cavity, the two cases differ. While boundary layer is still growing for the baseline case the by-pass mass flow, in the cavities case, sucked the boundary layer inside the inlet cavity. A new boundary layer is then created, thinner than in baseline case at the same axial position, and leads to passage vortex reduction.

Nevertheless, thanks to losses breakdown, the study also demonstrated that steady approach miss flow features especially the mixing process after the reintroduction. That is why, even if the influence of unsteadiness on loss generation is hard to quantify, discrepancy between RANS and URANS have to be investigated to get a better understanding of shrouded blades. The section hereafter uses instantaneous flow field from URANS simulations to describe influence

of shroud cavities on main flow.

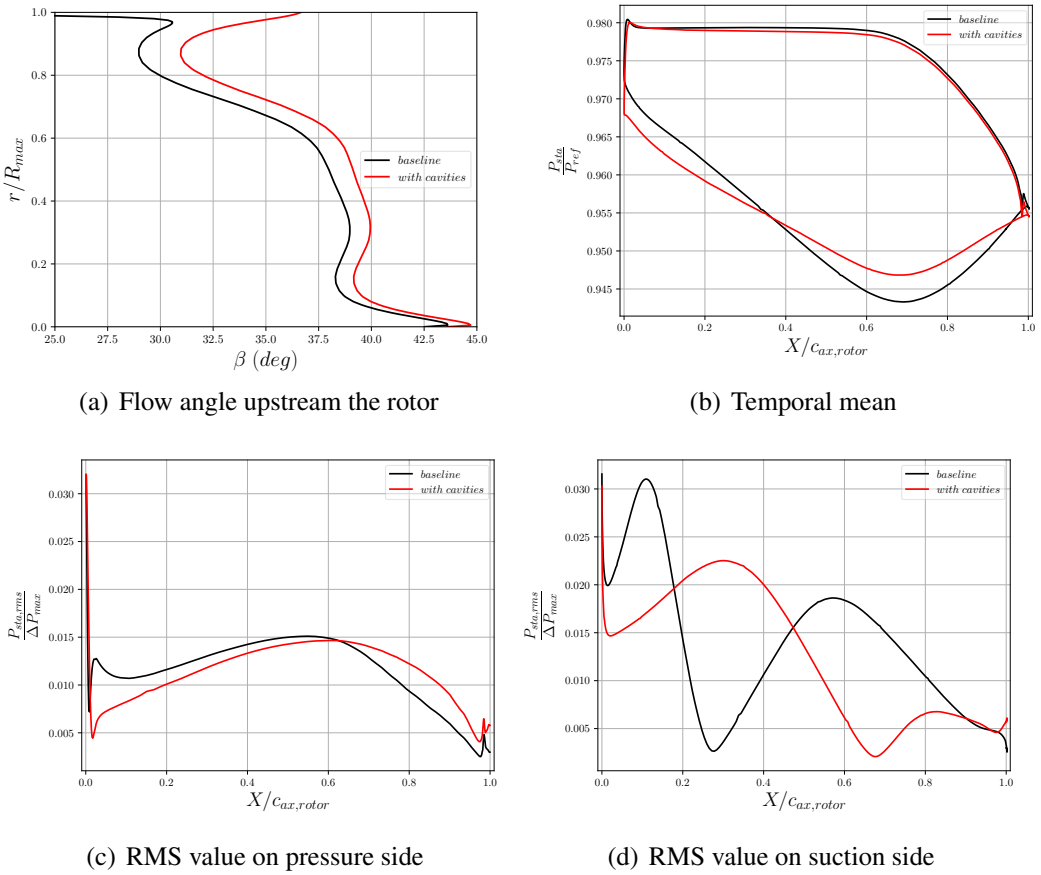

(a) Flow angle upstream the rotor

(b) Temporal mean

(c) RMS value on pressure side

(d) RMS value on suction side

Figure 6: **Flow angle upstream the rotor leading edge and static pressure profiles on rotor blade at 95% span for unsteady simulations**

Flow analysis

Figure 6 shows mean and RMS values of static pressure on rotor blade at 95% span for baseline and cavities cases. The static pressure around the blade is normalised using the reference value at the inlet of the domain. Fluctuations of static pressure are normalised using maximum variation of static pressure between extrados and intrados. The baseline case is represented with black line whereas cavities case with red lines. Both simulations target the same stage loading however the pressure distribution on the blades differs due to under-turning, above 80% of blade height, caused by shroud cavities. This under-turning is visible on Figure 6(a) representing radial profile of flow angle, in the relative frame of reference, in a plane $3mm$ upstream of the rotor leading edge. Shroud cavities also influence static pressure fluctuations on the blade. Contrary to the baseline case, the one with cavities has a reduction of fluctuations on suction side and a phase opposition between extrema. It comes from the fact that the by-pass mass flow suck up stator wake when it enters the inlet cavity. Wakes become distorted and impact rotor blades on the suction side at a slightly upstream position as shown on Figure 7. The figure represents a static pressure fluctuation field (RMS value) at 95% span with an iso-line of entropy, in black,

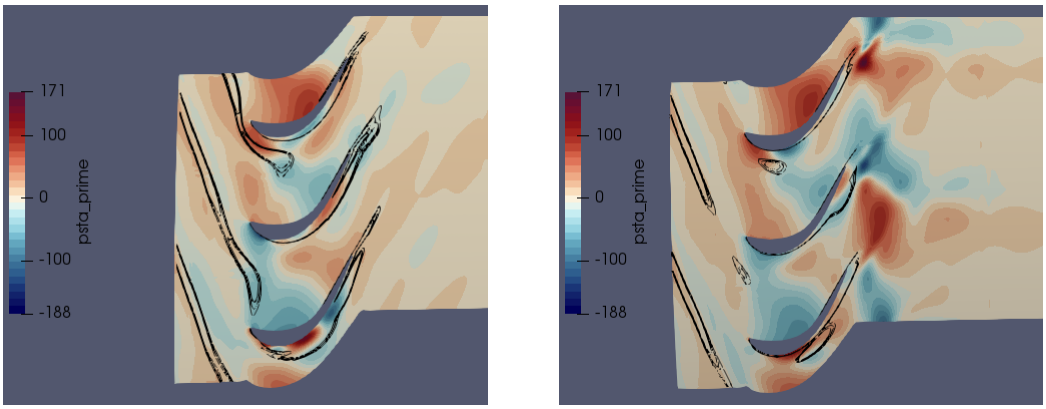

(a) Baseline (b) With cavities

Figure 7: **Representation of RMS value of static pressure on a cylindrical cut at 95% span. In black, iso-line of entropy.**

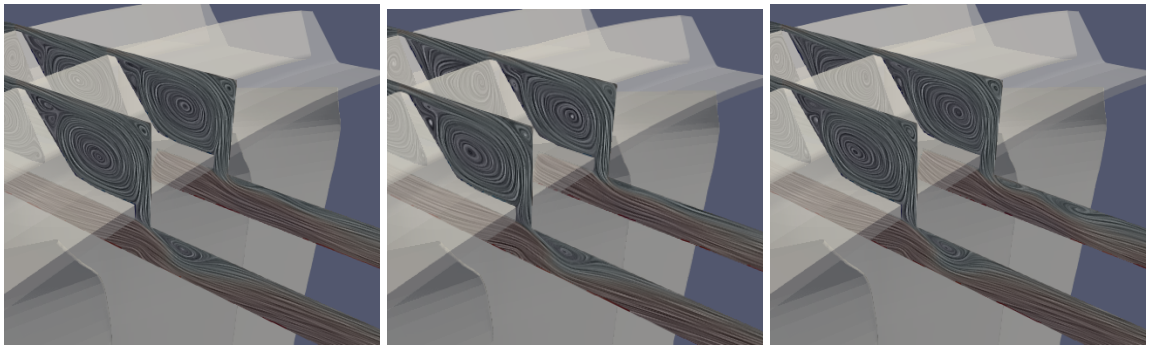

(a) RANS (b) Averaged URANS (c) Instantaneous URANS

Figure 8: **Relative velocity vector field representation on two planes at constant azimuth for RANS and URANS cavities cases**

defining stator wakes. In the baseline case stator wakes penetrate deepen in rotor channel than the other case. On pressure side, differences between the two cases are less significant. Shroud cavities reduce fluctuations on the first 60% of the rotor axial chord and then increase it. These observations have direct consequences on design phases. Indeed, the under-turning will clearly change work output and deteriorate downstream flow field. Also, a wrong prediction of blade loading may affect the operability of the rotor, especially regarding the allowed axial movement of the rotor relative to the casing in this region. At a different scale, pressure fluctuation may influence thermal transfer or boundary layer transition on rotor blade. To go further, use of large eddy simulation to evaluate the impact of these fluctuations on transition would be interesting.

The exit shroud cavity forces the by-pass mass flow to re-enter the main flow as a radial jet. This structure induces flow separation on shroud edge at the main flow / exit cavity interface. Figure 8 gives a representation of velocity vector field using ”line integral convolution” on two planes with constant azimuth, one on pressure side (foreground) and the other one on suction side (background). The separation bulb is visible downstream of the reintroduction. While

Table 3: **Global performance parameters**

	Design RANS	Design URANS	Off-design (Ps) RANS	Off-design (Ps) URANS	Off-design (Ω) RANS	Off-design (Ω) URANS
ψ	2.02	2.02	5.42	5.43	5.32	5.33
π_{tt}	1.04	1.04	1.14	1.14	1.03	1.03
M_r	0.19	0.19	0.43	0.43	0.20	0.20
η_{is}	0.905	0.902	0.812	0.803	0.800	0.791

vector fields are very similar between RANS and averaged URANS, the instantaneous vector field (Figure 8(c)) shows discrepancies on suction side plane. A second separation bulb appears and oscillates at the rotor blade passing frequency. The suction side of stator wake is convected through the rotor leading to periodically pressure drops in the outlet cavity region that support flow reintroduction. It generates additional losses and participates to flow angle modification on the downstream stage on 3% of the height. This is particularly important especially for industrial configuration with small inter row distances. Although the RANS approach is efficient to predict global performance, the present results show that analysis of unsteady mechanisms become necessary later in the design process. In addition, these mechanisms could be intensified at different operational condition.

Off-design condition

While turbofan turbines run close to design conditions for a significant part of their operational life time, multi-point (take off, climb and cruise) conditions are included during the design process. In addition, off-design condition may occur and may have a several impact on loss generation. Back pressure and rotational speed were changed to analyse their influence given the fact that these parameters are directly correlated to the pressure ratio across the fins, velocities differences between main flow and by-pass flow as well as unsteadiness. The configuration under consideration is lightly loaded thus modifications were done to increase stage loading. The back pressure was reduced by 10%, 15% and 20% compared to the design point and the rotational speed was reduced by 15%, 30% and 50%.

The paper will focus on the intermediate case regarding back pressure modification (-15%) and the most severe case for rotational speed (50%). The reason of this choice is led by the relatively close stage loading between these two cases $\psi_{Ps} = 5.4$ and $\psi_{\Omega} = 5.3$ respectively. Table 3 gives total-to-total pressure ration as well as Mach number at rotor exit for the two cases.

(U)RANS predictability

First of all, contrary to simulations at design conditions, there are significant difference on isentropic efficiency between RANS and URANS simulations. Table 3 summarised isentropic efficiency values for each simulations, at design and off-design conditions. At design condition the difference of 0.2 points corresponds to uncertainties during measurement on experimental facilities, according to Rosic et al. [14]. At off-design conditions differences are higher, thus more relevant, but the lack of experimental data does not permit to conclude whether or

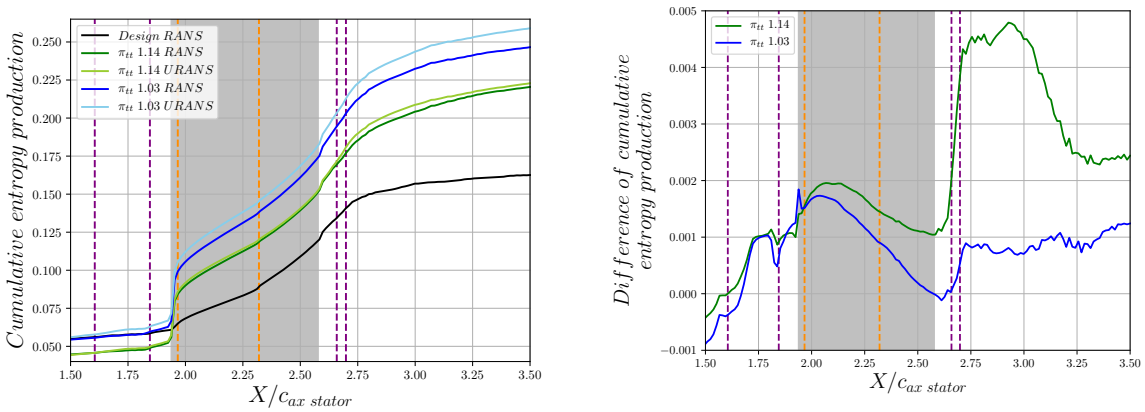

(a) All cases

(b) Difference RANS/URANS

Figure 9: **Cumulative entropy production along the turbine axis**

not URANS overestimate losses. Entropy production is plotted on Figure 9(a). The indirect method introduced by Zlatinov at al. [15] is used since actual mesh refinement does not ensure the validity of direct method. The cumulative entropy production is, in the present paper, normalised using kinetic energy at rotor outlet (MP03 plane, Fig. 9). Origin of x-axis is the stator leading edge but to get better visibility only the production inside rotor domain is shown. The vertical gray band represents the axial rotor chord, the two zones delimited by purple dashed lines correspond to inlet/outlet cavities and orange dashed line are the localisation of shroud fins. The RANS/URANS cases with higher and lower pressure ratio are represented by green curves and blue curves, respectivly. The black curve corresponds to the steady design configuration. For the higher pressure ratio case there is an inscrease of entropy production near the inlet cavity. Figure 9(b) gives the difference of entropy production between RANS and URANS simulations at off-design condition and helps for visualisation. However, the majority of change appears in the mixing process downstream the reintroduction of bypass mass flow. Indeed, the velocity increases both in the main flow and in the cavity thus differences in momentum at the reintroduction are amplified and an increase in mixing losses is expected. The results confirm the observed trend in [13] that RANS simulations underestimate mixing process. The lower pressure ratio case follows the same behaviour with amplified additional losses near the inlet cavity and after the reintroduction. Upstream the inlet cavity, curves for the RANS off-design ($\pi_{tt} = 1.03$) and RANS design cases are overlapping because velocity level are very similar. The level of entropy production for URANS off-design ($\pi_{tt} = 1.03$) is higher in this region and demonstrates the real influence of stator wakes upstream the rotor at this rotational speed.

Flow analysis

Figure 10 represents the radial component of velocity (V_r) at the interface between inlet cavity and rotor channel at design and for the two off-design conditions. An iso-line at $V_r = 0m/s$ is plotted in black to better visualise ingress ($V_r > 0$) and egress zones ($V_r < 0$). At design condition, egress zones are relatively small and the fluid exits the inlet cavity with small radial velocity ($-1 < V_r < 0$). The presence of the ingress/egress zones is one of the main flow feature described in the literature of tip shroud cavity. The fact that inlet cavity fluid hardly

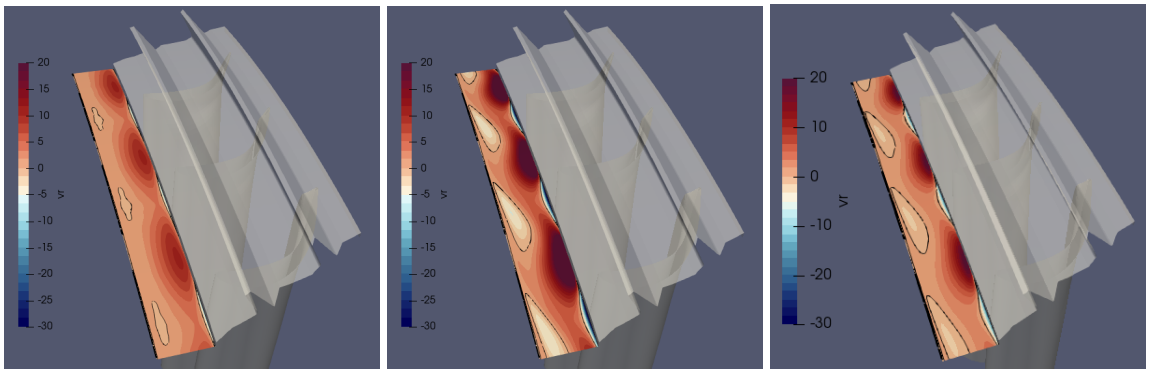

(a) Design condition (b) Off-design ($\pi_{tt} = 1.14$) (c) Off-design ($\pi_{tt} = 1.03$)

Figure 10: **Radial velocity field at inlet cavity interface from averaged URANS simulations at design and off-design conditions. Iso-line $V_r = 0$ in black**

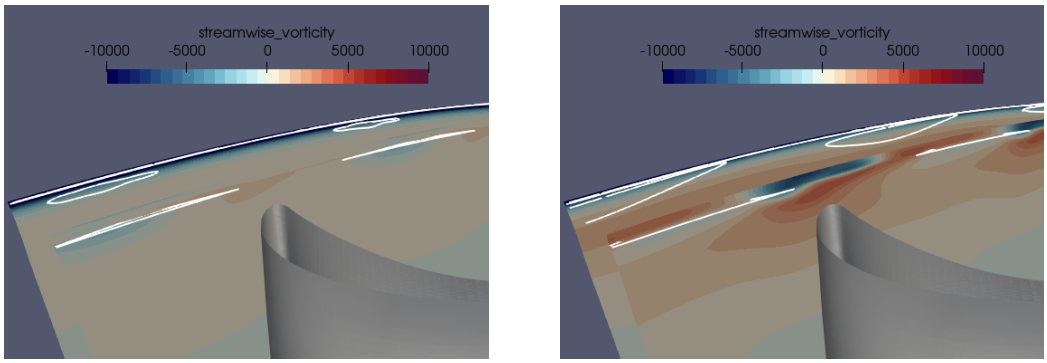

(a) Design condition (b) $\pi_{tt} = 1.14$

Figure 11: **Axial cuts of streamwise vorticity upstream rotor leading edge at design and off-design condition ($\pi_{tt} = 1.14$). In white, iso-line $V_r = 0$**

returns inside the main flow make the configuration very special. At off-design condition, with higher pressure ratio, egress zones are intensified ($-5 < V_r < 0$) and spread much more over the rotor channel. The averaged velocity at stator exit is multiplied by three at higher pressure ratio leading to stronger azimuthal gradient of static pressure upstream of rotor leading edge. It explains the observation since egress zones are found at local minima of static pressure. Regarding the case at lower pressure ratio, interactions between inlet cavity and main flow is half-way between the two previous cases. The pattern of egress zone is very similar to higher pressure ratio simulations however intensity is smaller due to velocity closer to design conditions. Anyway, the stage loading appears as a parameter in egress zones apparition. Change of egress and ingress zones along the azimuth generate axial vorticity as reported by Palmer [16]. Figure 11 represents streamwise component of vorticity in two axial cuts upstream and downstream inlet cavity interface at design and lower back pressure condition. Black lines are iso-lines of null radial velocity component at the interface. Contrary to the reference back pressure, induced axial vorticity by ingress/egress zones is clearly visible on Figure 11(b). It feeds the horseshoe

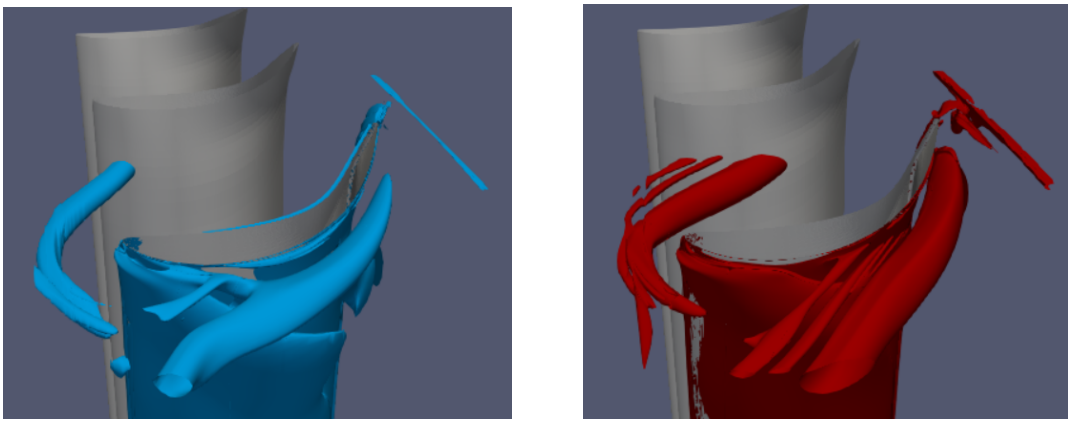

(a) Baseline (b) With cavities

Figure 12: **Iso-surface of Q-criterion in the rotor at** $\pi_{tt} = 1.14$

vortex originating at the rotor blade leading edge and intensifies secondary flows in the rotor. The lower pressure ratio case exhibit a similar behaviour but is not shown here. In order to distinguish the intensification due to over incidence and ingress/egress zones a simulation at off-design condition without cavities was done. Back pressure was slightly adapted in order to reach the same stage loading than with cavities. Figure 12 shows iso-surfaces of Q-criterion for the two higher pressure ratio cases, with and without cavities. The passage vortex is clearly more intense with cavities indicating that interaction between inlet cavity and main flow is also responsible for secondary flows intensification.

CONCLUSIONS

This paper presented a combined design and off design analysis of time resolved flow fields on low pressure turbine stage. Even if unsteady simulations do not seem necessary to predict the overall performance of the turbine stage, it help to better understand flow feature in vicinity of the shroud. At off-design conditions significant discrepancies appeared in the prediction of isentropic efficiency whether RANS or URANS simulations are run. Just as design condition, RANS simulations struggle to predict the mixing process downstream the reintroduction. In addition, at off-design conditions, interactions between inlet cavity and main flow appear due to stronger azimuthal pressure gradient and are intensified with stator wakes passages present in URANS simulations . The next step of the study is to extend the analysis to a multi stage configuration or at least with the downstream stator of the second stage.

References

[1] Sungho Yoon, Eric Curtis, John Denton, and John Longley. The effect of clearance on shrouded and unshrouded turbines at two levels of reaction. *Proceedings of the ASME Turbo Expo*, 7(PARTS A, B, AND C):1231–1241, 2010.

[2] Timothy R Palmer, Choon S Tan, Humberto Zuniga, David Little, Matthew Montgomery, and Anthony Malandra. Quantifying Loss Mechanisms in Turbine Tip Shroud Cavity Flows. *Journal of Turbomachinery*, 138(9):91006, 2016.

[3] Jochen Gier, Bertram Stubert, Bernard Brouillet, and Laurent de Vito. Interaction of shroud leakage flow and main flow in a three-stage LP turbine. *Journal of Turbomachinery*, 127(4):649–658, 2005.

[4] A Pfau, J Schlienger, D Rusch, A I Kalfas, and R S Abhari. Unsteady flow interactions within the inlet cavity of a turbine rotor tip labyrinth seal. In *ASME Turbo Expo 2003, collocated with the 2003 International Joint Power Generation Conference*, pages 187–199. American Society of Mechanical Engineers, 2003.

[5] Wei Jia and Huoxing Liu. Numerical investigation of the interaction between mainstream and tip shroud leakage flow in a 2-stage low pressure turbine. *Journal of Thermal Science*, 23(3):215–222, 2014.

[6] J D Denton et N.A Cumpsty. Loss mechanisms in turbomachines. *Journal of Turbomachinery. Transactions of the ASME*, 115(4):621–656, 1993.

[7] S Schrewe. *Experimental Investigation of the interaction between purge and main annulus flow upstream of a guide vane in a low pressure turbine*. PhD thesis, Université de Darmstadt, 2015.

[8] Stefan Zerobin, Andreas Peters, Sabine Bauinger, Ashwini Bhadravati Ramesh, Michael Steiner, Franz Heitmeir, and Emil Göttlich. Aerodynamic performance of turbine center frames with purge flows—part i: The influence of turbine purge flow rates. *Journal of Turbomachinery*, 140(6):061009, 2018.

[9] Johan C Kok. Resolving the dependence on freestream values for the k-turbulence model. *AIAA journal*, 38(7):1292–1295, 2000.

[10] J.R. Seume et al. L. Wein, T. Kluge. Validation of RANS turbulence models for labyrinth seal flows by mean of particule image velocimetry. *Proceedings of the ASME Turbo Expo*, 2020.

[11] Antony Jameson and Seokkwan Yoon. Lower-upper implicit schemes with multiple grids for the euler equations. *AIAA journal*, 25(7):929–935, 1987.

[12] Lars Wein, J R Seume, and F Herbst. Gpps-Na-2018-0036 Unsteady Flow in a Labyrinth Seal. 2018.

[13] Y. Bousquet M. Perini, N. Binder and E. Schwartz. Contribution of tip shroud cavity to loss generation in the main flow of a low pressure turbine using steady and unsteady numerical approach. *Proceedings of the ASME Turbo Expo*, 2020.

[14] Budimir Rosic, John D Denton, and Eric M Curtis. The influence of shroud and cavity geometry on turbine performance: an experimental and computational study—part I: shroud geometry. *Journal of Turbomachinery*, 130(4):41001, 2008.

[15] Metodi Blagoev Zlatinov, Choon Sooi Tan, Matthew Montgomery, Tito Islam, and Melissa Harris. Turbine hub and shroud sealing flow loss mechanisms. *Journal of Turbomachinery*, 134(6):61027, 2012.

[16] Timothy Richard Palmer. Effects of axial turbine tip shroud cavity flow on performance and durability. *PhD Thesis, Massachusetts Institute of Technology*, 2015.